One-Season to Five-Year Wetness/Dryness Outlooks: Data and Methods

By: Katherin Mendoza & Vikram Mehta

Data

The data used to construct the DCV indices was the Extended Reconstructed SST (ERSST; Reynolds et al. 2002). For the Tropical Atlantic sea-surface temperature Gradient (TAG) index, the ERSST was averaged over two regions- the tropical North (5°–20°N, 30°–60°W) and South (0°–20°S, 30°W–10°E) Atlantic Ocean- with the TAG index defined as the difference between the north and the south. The Pacific Decadal Oscillation (PDO) index was constructed from ERSST as defined by Mantua et al. (1997) as the normalized PC time series of the first EOF (Lorenz 1956) of the Pacific SST anomalies within the 20°N to 65°N, 125°E to 100°W domain. In order to remove the seasonal cycle, the respective monthly climatology from 1961 to 2010 was removed from both indices.

The Self-Calibrated Palmer Drought (SC-PDSI; Palmer 1965, Wells et al. 2004), the Standardized Precipitation Index (SPI; McKee et al. 1993), and the Standard Precipitation-Evapotranspiration Index (SPEI; Vicente-Serrano et al., 2010) are the three main drought indices available. The SC-PDSI is the most commonly used index using the local water balance. The SPI is based on the conversion of precipitation data to probabilities based on long-term precipitation records computed on different time scales. The SPEI combines the sensitivity to evaporation demand found with the SC-PDSI, and the simplicity of the SPI calculation at multiple time scales (Vicente-Serrano et al. 2012), and is therefore the data used for the dryness/wetness indicator in this study. The SPEI was constructed first by finding difference between the monthly precipitation and the potential evapotranspiration (PET) using the Thornthwaite equation (Thornthwaite 1948), then the resulting difference was aggregated and standardized using a 3-parameter distribution (Pearson III) at timescales from 1 to 24 months. Global correlations were calculated with each SPEI timescale and the SC-PDSI to determine the timescale used. The 9-month SPEI timescale was selected based on larger global correlations with the SC-PDSI. Any location that was missing more than 20% of the data for the given time period used was removed from the analysis.

Methods

DCV phenomena historically tend to stay in phase on average from 8 to 10 years, therefore, persistence is a strong indicator of phase transitions from season to season and year to year. However, when the DCV change phase the dryness/wetness across the world is effected. In order to predict the phase DCV phenomena in the future, we looked to the past. First, transition probabilities of phase (+ above zero, and – below zero) were calculated for each index. The transition probabilities between phases with lead times of one to four seasons, and one to five years, were created using DCV data from 1951 through 2017. The transition probabilities were created between each timescale phases from 1951 to the season (year) one year prior to make the prediction. For example to predict September to November 2008 with a two-season lead time, transition probabilities from March to May 1951 to September to November 2007 where used, along with the actual March to May 2008 DCV phases. Table 1 shows the accuracy of the predicted the sign both PDO and TAG using one-season to five-year lead time for roughly the last three decades (1992 to 2018) and the last decade (2008 to 2018). Both PDO and TAG are

accuracy predicted with significance (more than by chance- 50%) at nearly all lead times. The prediction of the DCV signs over the last decade were just as accurate, or more accurate as the last three decades, therefore only the last decade- 2008 to 2018- will be used in the following analysis.

Next, the two DCVs' phases were combined resulting in four possible phase combinations: PDO+ TAG+, PDO+ TAG-, PDO- TAG+, PDO- TAG-. The two DCV phase transition probabilities with one-season to five-year lead times were calculated and used to produce the seasonal (yearly) dryness/wetness outlooks. The largest transition probability was used to determine the predicted DCV phases. If more than one transition probability had the largest value, the transition that was most similar to the actual DCV phases of the predictor year was selected. For one-season to two-year lead times this was always the same phase transition probability, however, for three-year to five-year lead times the same phase transition probability was not always the largest.

In order to produce the dryness/wetness outlooks using the transition probabilities, composites of the SPEI were created using the historical DCV phases from the same time period used to create the transition probabilities (from 1951 to the year prior to the year of the prediction) for each of the four combined DCV phases. Years corresponding to each phase combination were averaged to create a DCV phase composite of SPEI values. Only the phase of the SPEI was determined resulting in values of either negative (dryness) or positive (wetness) regardless of the magnitude.

Finally, the DCV predicted phases and the composites were used together to create the dryness/wetness outlooks. The composite of SPEI associated with the same DCV phases of the predicted DCV phases with the largest transition probability was used as the outlook. This was done with lead times of one season to five years.

In order to find the accuracy of the dryness/wetness outlooks, outlooks from 2008 to 2018 were found and compared with the sign of the actual SPEI values for the outlook year. An outlook was defined as accurate in locations where the sign of the SPEI matched the sign of the outlook. The accurate locations from the eleven verification years where then counted and made into probability (percent) of accuracy values. (i.e. if a location was accurate 8 out of the 11 years the probability would be [8/11]*100=73%). Figure 1 shows the probability of accuracy for the one-season lead time. The outlook accuracy would be 50% each for dryness and wetness if they were equally probable, therefore, only regions which had a better than 50% probability of correct outlook are plotted. As figure 1 shows, one-season lead time results are very robust across the world for all four seasons. Southern U.S. has accuracy probabilities between 70-90% for three of the four seasons with 50-60% in the remaining season. September-October-November has 80-100% accuracy in western Africa, a region very susceptible to drought; southern Africa has large accuracy probabilities from March to August during the dry season. Large areas of accuracy are found in northern South America from March to August, and more localized areas of accuracy through November. North eastern Australia consistently has 60-90% accuracy in all four seasons with the rest of northern Australia having accuracy in March to May. The one-year lead time probability of accuracy figure (not shown) has the same regions, southeastern U.S., western and southern Africa, northern South America, and northeastern Australia with 60-90% or more. As the lead time increases, the regions of high accuracy fluctuate. Figure 2 shows the probability of

accuracy for the two- to five-year lead times. In Figure 2a northern Brazil, southern Africa, and all of Australia are areas with large accuracy probabilities with a two-year lead time. The three-year lead time (figure 2b) has localized high probabilities in northern mid-latitude, with larger areas of higher probability in southern mid-latitudes. Figure 2c (four-year lead time) depicts tropical latitudes worldwide show regions of high (90-100%) accuracy, and regions in mid-latitude locations such as Australia, northeast U.S., and Spain all have accuracy of 60-90%. A five-year lead time (figure 2d) also has areas of large accuracy in the topical latitudes, although not as large as the four-year lead time. From the worldwide analysis of the verification of the dryness/wetness outlooks, four regions (eastern U.S., northern South America, western Africa, and eastern Australia) were selected to provide a detailed analysis of the results including seasonal and annual outlooks from 2019 to 2023.

Table 1. Prediction accuracy (%) of sign of DCV by lead time from 1992 to 2018 and from 2008 to 2018. Bold values indicate significance.

		1992 - 2018		2008 - 2018	
Lead Time		PDO	TAG	PDO	TAG
One-Season	DJF to MAM	**59**	48	**55**	**55**
	MAM to JJA	**74**	**52**	**82**	**55**
	JJA to SON	**52**	48	**64**	45
	SON to DJF	**89**	**74**	**91**	**64**
Two-Season	DJF to JJA	**63**	44	**73**	**55**
	MAM to SON	**52**	**52**	**64**	**55**
	JJA to DJF	**70**	**63**	**82**	**55**
	SON to MAM	**89**	**52**	**91**	**55**
Three-Season	DJF to SON	48	**74**	**55**	**91**
	MAM to DJF	**70**	**67**	**82**	**64**
	JJA to MAM	**70**	48	**64**	**64**
	SON to JJA	**70**	37	**73**	**55**
Four-Season	DJF to DJF	**59**	**56**	**73**	**55**
	MAM to MAM	**70**	**56**	**64**	**55**
	JJA to JJA	**81**	48	**82**	45
	SON to SON	**59**	**63**	**55**	**82**
One-Year		**81**	41	**91**	36
Two-Year		**63**	**56**	**73**	**55**
Three-Year		44	44	**55**	36
Four-Year		**74**	**56**	**64**	**55**
Five-Year		48	**59**	**55**	**73**

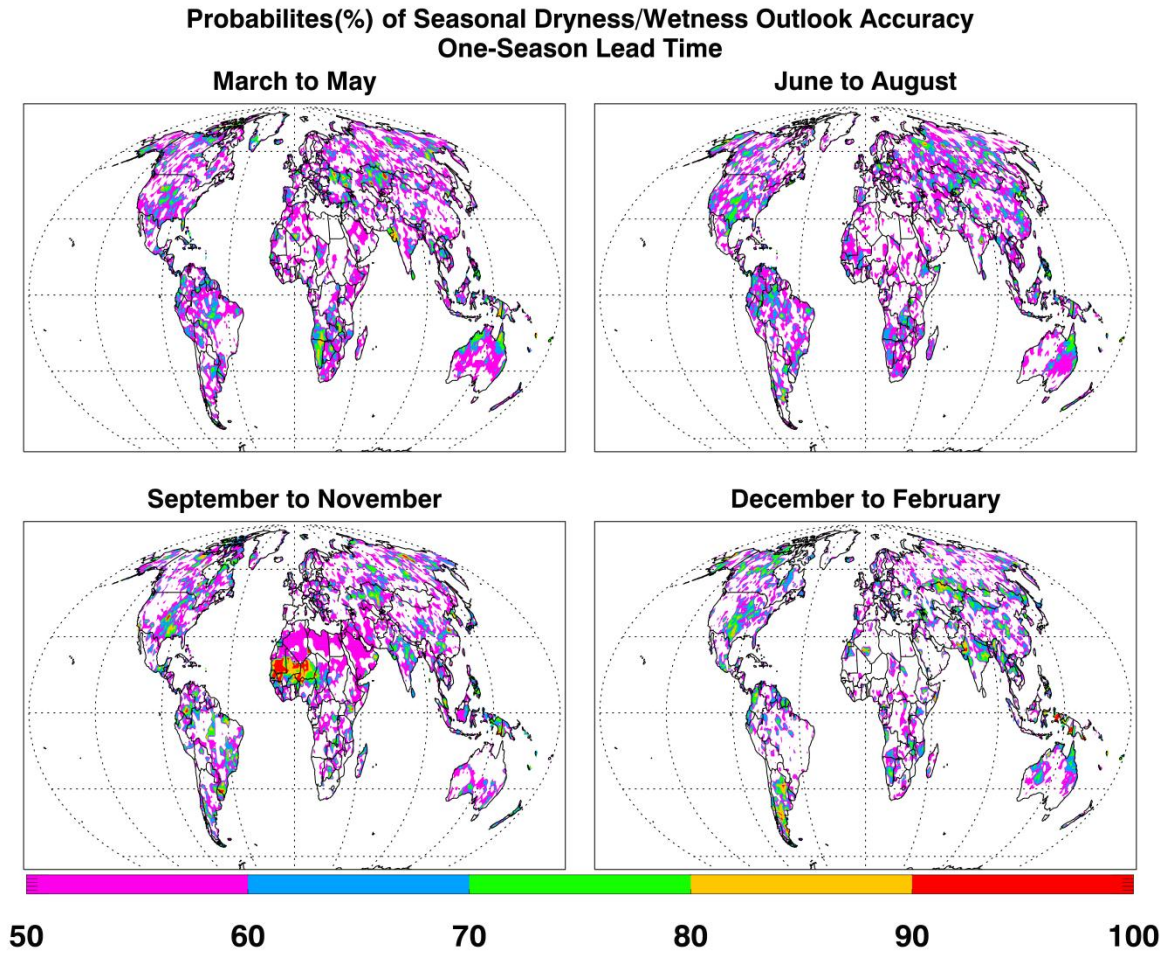

Figure 1. The probability of accuracy of dryness/wetness outlooks from 2008 to 2018 for outlooks made with one-season lead time. Only areas of greater than 50% accuracy are plotted.

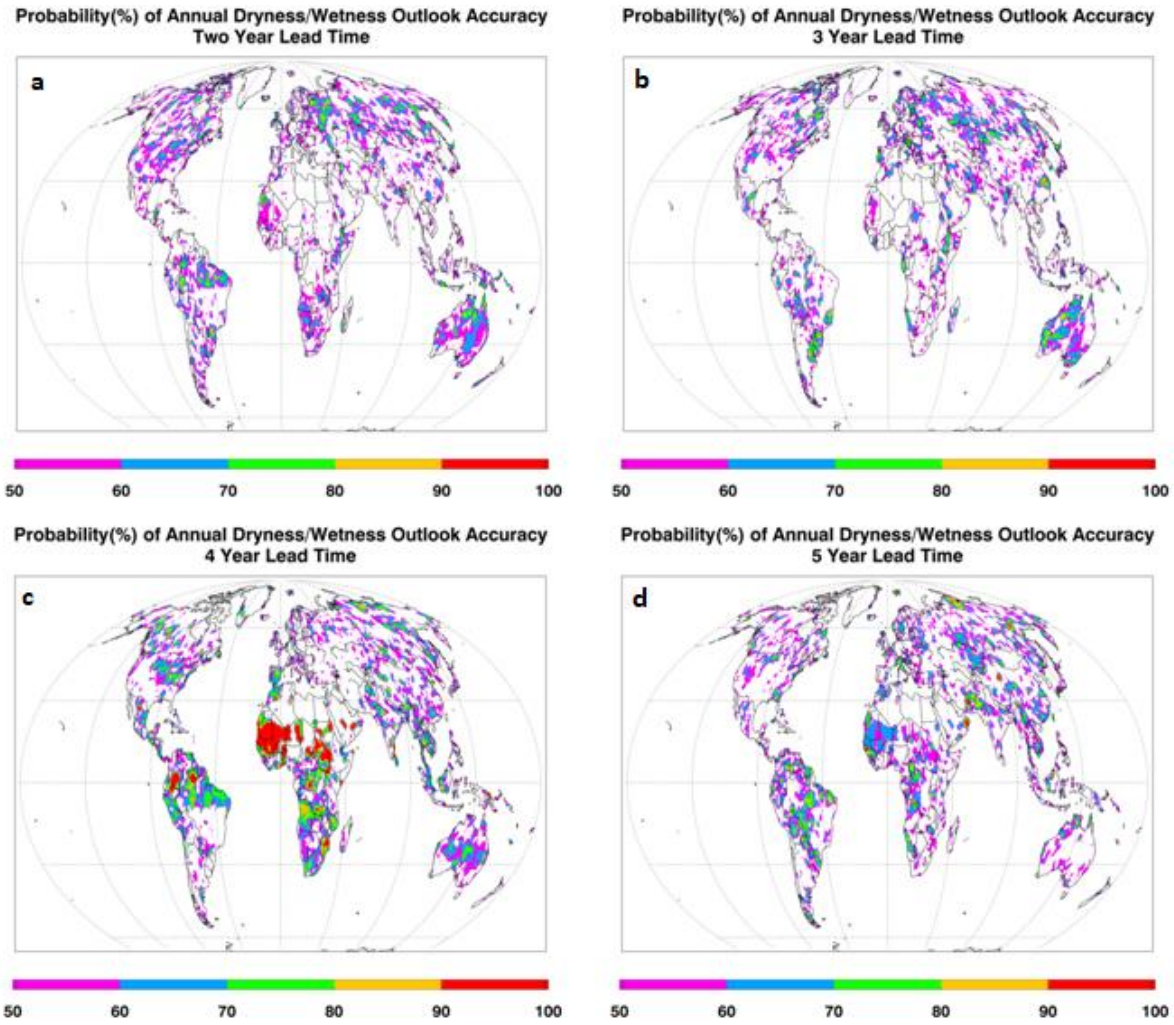

Figure 2. The probability of accuracy of dryness/wetness outlooks from 2008 to 2018 for outlooks made with (a) two-year, (b) three-year, (c) four-year, and (d) five-year lead time. Only areas of greater than 50% accuracy are plotted.

References

Lorenz E.N., 1956. Empirical orthogonal functions and statistical weather prediction. MIT, Dept of Meteorology Science Report 1:49.

Mantua NJ, Hare SR, Zhang Y, Wallace JM, Francis RC, 1997. A Pacific interdecadal climate oscillation with impacts on salmon production. Bull Amer Meteorol Soc 78:1069–1079.

McKee, T. B. N., J. Doesken, and J. Kleist, 1993: The relationship of drought frequency and duration to time scales. Proc. Eight Conf. on Applied Climatology. Anaheim, CA, Amer. Meteor. Soc. 179–184.

Palmer, W. C., 1965: Meteorological droughts. U.S. Department of Commerce Weather Bureau Research Paper 45, 58 pp.

Reynolds RW, Rayner NA, Smith TM, Stokes DC, Wang W, 2002. An improved in situ and satellite SST analysis for climate. J Clim 15:1609–1625.

Thornthwaite, C. W., 1948: An approach toward a rational classification of climate. Geogr. Rev., 38, 55–94.

Vicente-Serrano, S. M., S. Beguería, and J. I. Lopez-Moreno, 2010: A multiscalar drought index sensitive to global warming: The standardized precipitation evapotranspiration index. J. Climate, 23, 1696–1718.

Vicente-Serrano, S.M., Beguería, S., Lorenzo-Lacruz, J., et al., 2012: Performance of drought indices for ecological, agricultural and hydrological applications. Earth Interactions 16, 1–27.

Wells, N., S. Goddard, and M. J. Hayes, 2004: A self-calibrating Palmer drought severity index. J. Climate, 17, 2335–2351.